Mar Syst Ocean Technol (2015) 10:60–70
DOI 10.1007/s40868-015-0005-4

Experimental validation of relationship between fracture parameters *J* and CTOD for SE(B) and SE(T) specimens during ductile crack growth

Diego F. B. Sarzosa[1] · **Claudio Ruggieri**[1]

Received: 17 December 2014 / Accepted: 23 April 2015 / Published online: 11 June 2015

Abstract In structural assessments, the crack driving force is usually estimated numerically based on the *J*-Integral definition because its determination is well established in many finite element codes. The nuclear industry has extensive fracture toughness data expressed in terms of *J*-Integral and huge experience with its applications and limitations. On the other hand, the material fracture toughness is typically measured by CTOD parameter using the plastic hinge model or double-clip gauge technique. The parameter CTOD has a wide acceptance in the Oil and Gas Industry (OGI). Also, the OGI has a lot of past data expressed in terms of CTOD, and the people involved are very familiar with this parameter. Furthermore, CTOD parameter is based on the physical deformation of the crack faces and can be visualized and understood in an easy way. There is a unique relationship between *J* and CTOD beyond the validity limits of linear elastic fracture mechanics for stationary cracks. However, if ductile crack propagation happens, the crack tip deformation profile and stress–strain fields ahead of the crack tip will change significantly when compared to the static case. Thus, the stable crack propagation may change the well-established relationship between *J* and CTOD for stationary cracks compromising the construction of resistance curves J-Δa from CTOD-Δa data or vice versa. A search in the open literature was undertaken to get experimental measurements of *J*-Integral and CTOD data including ductile crack growth. Then, using theoretical relations developed in previous work, predictions for CTOD values from *J* values are performed and directly compared with the experimental values. The present results provide additional understanding of the effects of ductile crack growth on the relationship between *J*-Integral and CTOD for standard fracture specimens. Specific procedures for the evaluation of CTOD-R curves using SE(T) and SE(B) specimens are proposed.

Keywords CTOD · *J*-integral · Ductile crack growth fracture toughness · ECA

1 Introduction

The Oil and Gas Industry has some bias to use crack tip opening displacement (CTOD) as the parameter to describe fracture toughness data [1]. On the other hand, crack driving forces can be easily characterized by *J*-Integral using finite element analysis. Both parameters have advantages and disadvantages. First, *J*-Integral parameter has a robust mathematical definition, and its determination is well established in all major commercial finite element codes. However, the *J*-Integral dominance breaks down when excessive plasticity (large strain) spreads over the remaining ligament.

Second, CTOD parameter is based on the physical deformation of the crack faces and can be visualized and understood in an easy way . Theoretically, it does not have mathematical limitations regarding the level of plastic deformation ahead of the crack tip or elastic unloading associated with crack growth or stress–strain relationship. Also, since CTOD is a physical parameter, it is often regarded as a simple, quantitative measure of material toughness. The value of crack tip displacement increases in proportion to the toughness of the material [2].

✉ Diego F. B. Sarzosa
dsarzosa@usp.br

Claudio Ruggieri
claudio.ruggieri@usp.br

[1] Department of Naval Architecture and Ocean Engineering, University of São Paulo, São Paulo, Brazil

CTOD parameter has no unique definition, that is, there is no single crack face displacement that can be regarded as characteristic property of the material. Also, the plastic hinge model typically used to measure CTOD assumes that crack faces remain straight, allowing the use of similar triangles to calculate CTOD. It is not valid for materials with high hardening, low levels of plastic displacements, and shallow cracks [3].

Currently, the American standard ASTM E1820-13 [4] defines the relationship between J-Integral and *CTOD* via an empirical plastic constraint factor (m). This m factor is expressed as function of the crack size (a/W) and a measure of the strain-hardening capacity defined by the ratio $\frac{\sigma_{ys}}{\sigma_{uts}}$, where σ_{ys} is the yield strength and σ_{uts} is the ultimate tensile strength.

Recently, the American Society for Testing and Materials (ASTM) substantially modified its methodology for assessing the parameter *CTOD* in its procedures ASTM E1290-08 [5] (and, consequently, also the ASTM E1820-08 [4]) using specimens SE(B) and C(T). The current approach is now based on the determination of the J-Integral (usually through the plastic work approach using load versus displacement measurements—CMOD or LLD) followed by its conversion to a corresponding value of CTOD. Therefore, as a material fracture toughness property, J parameter is measured using the area under the load–displacement curve (U), so J is directly proportional to U. In contrast, according to the plastic hinge model, δ is proportional to plastic component of the mouth opening displacement. Thus, the relationship between both parameters depends on strain hardening and the level of crack tip constraint [6].

Shih [7] showed a unique relationship exists between J and *CTOD* beyond the validity limits of linear elastic fracture mechanics (LEFM). Rice by a private communication suggested an operational definition of the crack tip opening displacement as the opening distance between the intercept of two 45°-lines, drawn back from the tip with the deformed profile as illustrated in Fig. 1a.

Shih using the HHR singularity to estimate the crack tip displacements obtained the following relation [7]:

$$\delta = d_n \frac{J}{\sigma_{YS}} \tag{1}$$

where δ is the crack tip opening displacement, σ_{YS} is the yield stress, and d_n is a dimensionless constant that is related to m $(d_n = 1/m)$.

Shih [7] stated that a unique relationship between J and δ, as defined by Eq. (1), requires that the HHR field dominates the crack tip deformation over a size scale at least of the order of one CTOD . The annular sector size $\bar{R}$ where the HHR singularity dominated decreases for low hardening materials and vanishes in the limit of non-

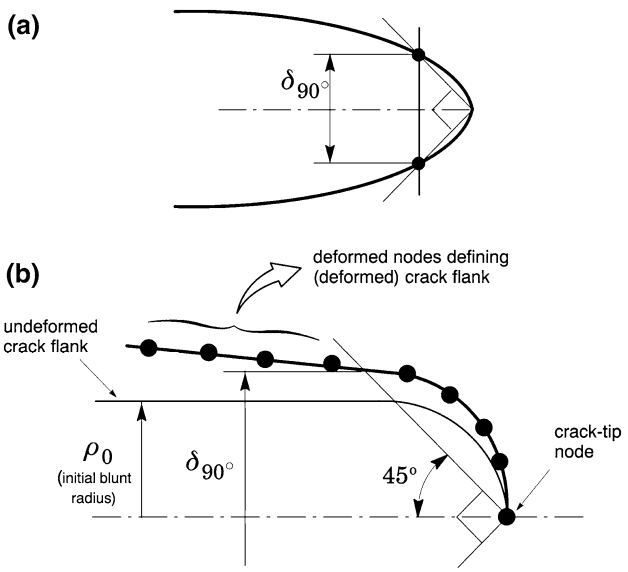

Fig. 1 **a** Definition of CTOD based on the 90° intercept procedure; **b** adopted numerical strategy to evaluate the CTOD

hardening material. Therefore, a unique relationship between J and δ may not exist for non-hardening material. In contrast, for hardening materials in SSY condition, a unique relationship between J and δ has been proven to exist. Under large-scale yielding (LSY), the work of McMeeking and Parks [8] and Shih and German [9] showed that the size of the HHR singularity-dominated zone is dependent on specimen geometry. Specifically, they showed that specimens under pure bending have larger dominated zones by the HHR fields than specimens under tension for fully plastic conditions. According to Shih [7], these results indicate that Eq. (1) may continue to hold for hardening materials subjected primarily to bending under LSY and may not be valid for ligaments subjected primarily to tensile loading.

Engineering critical assessment (ECA) procedures applicable to reeled pipes [10] rely on direct applications of $J(CTOD)$ resistance data measured using small, laboratory fracture specimens to specify acceptable flaw sizes. These approaches allow the specification of critical crack sizes based on the predicted growth of crack-like defects under service conditions. Current standardization efforts now underway [11–13] advocate the use of single-edge notch tension specimens (often termed SE(T) or SENT crack configurations) to measure experimental R-curves more applicable to high-pressure piping systems and girth welds of marine steel risers. The primary motivation to use SE(T) specimens to describe the fracture toughness curve is the similarity in the crack tip fields (stresses and strains), which control the fracture process, between the SE(T) geometry and pipeline girth welds under bending as SINTEF's work showed [14]. It is worthy to mention that the SE(T)

specimen has been included in the British Standard BS8571:2014 [15] as reference geometry to measure fracture toughness in metallic materials in terms of δ and J parameters.

The SE(T) geometry generally develops low levels of crack tip stress triaxiality (associated with the predominant tensile loading which develops during the fracture test) thereby contrasting sharply to conditions present in deeply cracked SE(B) and C(T) fracture specimens. Recent applications of SE(T) fracture specimens to characterize crack growth resistance properties in pipeline steels [16] have been effective in providing larger flaw tolerances while, at the same time, reducing the otherwise excessive conservatism which arises when measuring the material's fracture toughness based on high constraint, deeply cracked SE(B) specimens. However, crack growth effect on specimen's constraint and its implications for ECA analysis have not been evaluated exhaustively. The stable crack propagation may change the well-established relationship, under small-scale yielding (SSY) conditions, between J and $CTOD$ [7] for stationary cracks compromising the construction of resistance curves $CTOD - \triangle a$ from the determination of J-Integral. Therefore, during fracture assessments of critical structures, including piping and marine facilities, it is necessary to know accurate relationships between the J-Integral and CTOD parameters.

Although conceptually simple and directly connected with fundamental methodologies for determining the J Integral (such as η methodology [11, 17, 18]), there are no J versus δ relations specifically developed for SE(T) specimens or reeled pipelines. Perhaps more importantly, few and limited relationships between J and $CTOD$ available in the scientific and technical literature do not explicitly consider the evolution of $CTOD$ when the crack is under stable propagation mode I. Indeed, as illustrated schematically in Fig. 2, the ductile crack extension changes the crack tip profile, and it has a great impact on the correct definition of $CTOD$. Also, Fig. 2 shows possible definitions to measure $CTOD$ for growing cracks. One definition of CTOD (Fig. 2, left) measures the vertical displacement using the 90° definition at the original crack tip. The second definition (Fig. 2, right) uses the displacement of the crack faces remote from the tip to define the slope of a line that is going to help define the CTOD at the current crack tip [19]. This line is extrapolated, and its intercept with a vertical line at the current crack tip defines $\delta/2$.

This research study provides experimental checking of previously developed [20] m-equations, i.e., J and $CTOD(\delta)$ relationships, for SEN(T) and SE(B) specimens. The main goal was to verify the robustness of the comprehensive set of expressions between J and δ for SEN(T) and SE(B) geometries commonly use to obtain resistance $CTOD$-R curves from J-R curves or vice versa as specified in testing protocols for toughness measurements.

2 Experimental procedure for measuring J and CTOD values

Regarding the experimental data, all information has been taken from [21–24]. This section describes the experimental procedure used in [21, 22] to estimate δ and J-Integral values from their laboratory tests. It was possible to find open data for SE(B) and SE(T) geometries.

2.1 J Estimation procedure based on plastic work

Evaluation of the J-integral from laboratory measurements of load–displacement records is most often accomplished by considering the elastic and plastic contributions to the strain energy for a cracked body under Mode I deformation [2] as follows

$$J = J_e + J_p \tag{2}$$

where the elastic component, J_e, is given by the standard form

$$J_e = \frac{K_I^2}{E'} \tag{3}$$

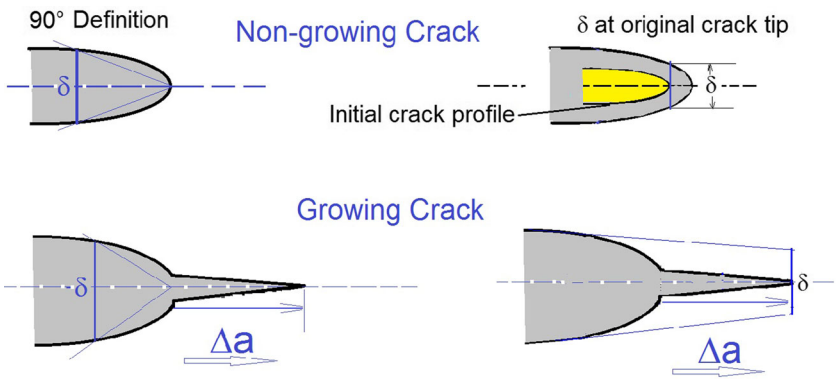

Fig. 2 Illustration of possible definitions of CTOD for growing cracks

in which K_I is the (Mode I) elastic stress intensity factor and $E' = E$ or $E' = E/(1-\nu^2)$ whether plane stress or plane-strain conditions are assumed with E representing the elastic modulus. Here, solutions for the elastic stress intensity factor, K_I , for a SE(B) specimen are given by Tada et al. [25] whereas Cravero and Ruggieri [26] provide wide range K_I-solutions for pin-loaded and clamped SE(T) specimens.

The plastic component, J_p, is conveniently evaluated from the plastic area under the load–CMOD curve as

$$J_p = \frac{\eta_J A_p}{bB} \tag{4}$$

where A_p is the plastic area under the load–CMOD curve, and factor η_J represents a non-dimensional parameter which describes the effect of plastic strain energy on the applied J. The previous definition for J_p derives from the assumption of nonlinear elastic material response thereby providing a deformation plasticity quantity. Figure 3 schematically illustrates the procedure to determine the plastic area to calculate J from typical load–CMOD records in which the crack mouth opening displacement is often also denoted V. All experimental J values have been evaluated using the K and η equations given in DNV-RP-F108 [12]. Therefore, no crack growth correction has been considered in J values, and as the procedure explains, a correction factor of 0.85 is included in η factor equations to take into account the uncertain effects of work hardening and weld metal strength mismatch.

2.2 CTOD evaluation procedure

The previous framework also applies when the CTOD is adopted to characterize the crack tip driving force. Following the earlier analysis for the J-integral and using the connection between J and the crack tip opening displacement (δ), given by Eq. (1), yield the following relationship:

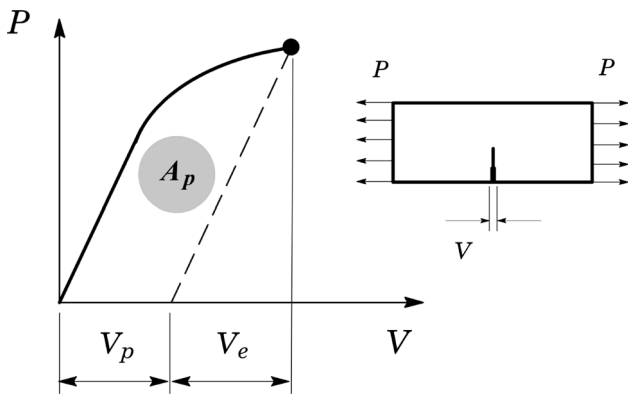

Fig. 3 Plastic area under the load–displacement (CMOD) curve for a fracture specimen

$$\delta = \delta_e + \delta_p \tag{5}$$

where the elastic component, δ_e, is given by

$$\delta_e = \frac{K_I^2}{m_{SSY}\sigma_{ys}E'}, \tag{6}$$

and the plastic component, δ_p, is expressed as

$$\delta_p = \frac{\eta_\delta A_p}{bB\sigma_{ys}} \tag{7}$$

where factor η_δ now represents a non-dimensional parameter which describes the effect of plastic strain energy on the applied CTOD. In the above expressions, m_{SSY} is a plastic constraint factor relating J and CTOD under small-scale yielding [2], σ_{ys} denotes the material's yield stress, and parameter m represents a proportionality coefficient often used to relate the total value of J to the total value of CTOD which strongly depends on the material's strain hardening [7, 27]. The η_δ factors were reported for SE(B) and clamped SE(T) geometries in previous work [20].

Despite being a straightforward procedure to calculate CTOD from laboratory measurements of load–displacement records, a much simpler and direct protocol has been followed by world researchers, see [21–24], using a couple of clip gauges mounted above the crack mouth and making trigonometric relations with the δ displacement near the crack tip as follows:

$$\delta = V_1 - \frac{a_0 + z_1}{z_2 - z_1}(V_2 - V_1) \tag{8}$$

where V_1 and V_2 are the lower and upper clip gauge readings, a_0 is the initial crack size, and z_1 and z_2 are the heights of the lower and upper knife edges above the specimen surface.

3 Numerical procedures

3.1 Finite element models for stationary crack analyses

In previous work [20], nonlinear finite element analyses were carried out for plane-strain models of bend and tension loaded crack configurations covering 1-T plane-sided SE(B) and SE(T) fracture specimens with fixed overall geometry having thickness $B = 1$ mm and varying crack sizes. It should be indicated that the finite element code WARP3D [28] used to solve the problem only support 3D elements. Thus, the plane-strain condition is achieved by preventing the out-of-plane displacements at all nodes in the finite element model. The analysis matrix includes standard SE(B) specimens ($S/W = 4$) and clamped SE(T) specimens ($H/W = 10$) with $W/B = 2$ having $a/W = 0.10$ to 0.7 with increments of 0.05. Here, a is the crack

size, W is the specimen width, S defines the specimen span for the bend configuration, and H represents the distance between clamps for the tension specimen. Figure 4 shows the geometry and specimen dimensions for the analyzed crack configurations.

Figure 5 shows the finite element models constructed for the plane-strain analyses of the clamped SE(T) specimen having $a/W = 0.5$ for stationary crack analysis. All other crack models have very similar features. A conventional mesh configuration having a focused ring of elements surrounding the crack front is used with a small keyhole at the crack tip; the radius of the keyhole, ρ_0, is 2.5 μm (0.0025 mm) to enhance computation of J-values at low deformation levels. Previous numerical analyses [26] reveal that such mesh design provides detailed resolution of the near-tip stress–strain fields which is needed for accurate numerical evaluation of J-values. Symmetry conditions permit modeling of only one-half of the specimen with appropriate constraints imposed on the remaining ligament. A typical half-symmetric model has one thickness layer of 1300 8-node, 3D elements ($\sim$2800 nodes) with plane-strain constraints (prevention of deformation out-of-plane $w = 0$) imposed on each node. These finite element models are loaded by displacement increments imposed on the loading points to enhance numerical convergence.

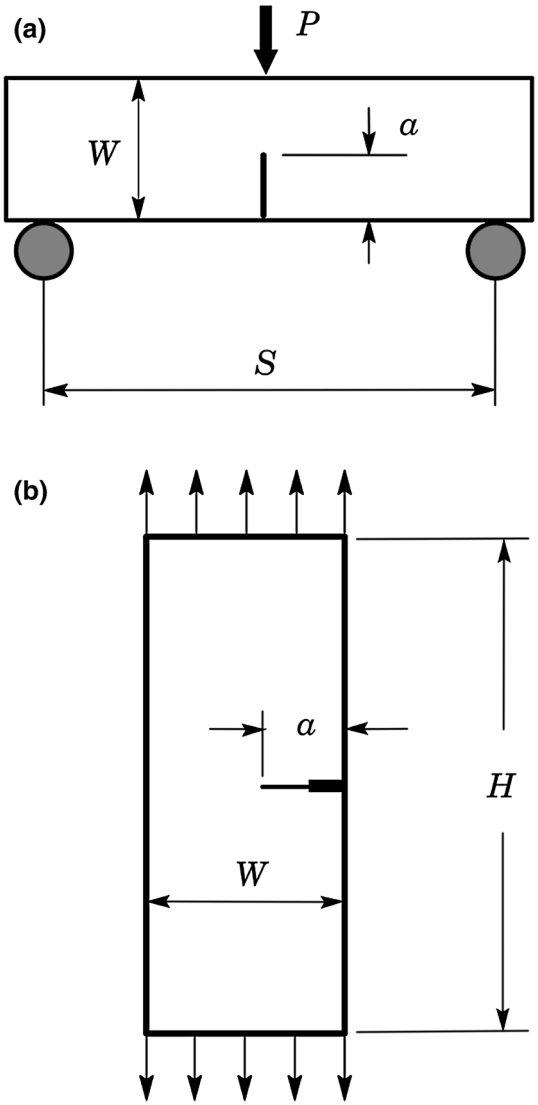

Fig. 4 Specimen geometries and dimensions for analyzed crack configurations

The elastic–plastic constitutive model employed in the stationary crack analyses reported in [20] follows a flow theory with conventional Mises plasticity in small geometry change (SGC) setting. The numerical solutions for fracture specimens and cracked pipes utilize a simple power-hardening model to characterize the uniaxial true stress ($\bar{\sigma}$) versus logarithmic strain ($\bar{\epsilon}$) in the form

$$\frac{\bar{\epsilon}}{\epsilon_0} = \frac{\bar{\sigma}}{\sigma_0}\ ,\ \epsilon \le \epsilon_0\ ;\ \frac{\bar{\epsilon}}{\epsilon_0} = \left(\frac{\bar{\sigma}}{\sigma_0}\right)^n\ ,\ \epsilon > \epsilon_0 \tag{9}$$

where σ_0 and ϵ_0 are the reference (yield) stress and strain, and n is the strain-hardening exponent. The finite element analyses consider material flow properties covering typical structural, pressure vessel, and pipeline grade steels with $E = 206$ GPa and $v = 0.3 : n = 5$ and $E/\sigma_{ys} = 800$ (high hardening material), $n = 10$ and $E/\sigma_{ys} = 500$ (moderate hardening material) and $n = 20$ and $E/\sigma_{ys} = 300$ (low hardening material).

The finite element code WARP3D [28] was used to solve the numerical equations for the plane-strain simulations reported in [20] and reproduced here. The research code FRACTUS2D [29] was employed to compute CTOD values δ for the SE(B) and clamped SE(T) specimens, and the $J-$CTOD relationships derived from stationary analyses for the analyzed fracture specimens. Evaluation of the numerical value of CTOD follows the 90° procedure [2] to the deformed crack flanks. To avoid potential problems with the CTOD computation related to the severe mesh deformation at the crack tip, the approach adopted here defines the value of half the crack tip opening displacement as the intercept between a straight line at 45° from the initial crack tip for stationary analyses and from the current and initial crack tip for crack growth analyses and a straight line passing through selected nodes at the crack flank as illustrated in Fig. 1b. The straight line defined by the deformed crack flank nodes is obtained by a linear regression of the corresponding nodal displacements.

Figure 6 illustrates the numerical procedure to determine the value of parameter m. A regression analyses is performed to obtain the best fit to the numerical data ($CTOD_i$, J_i/σ_{flow}). It should be noted that there is a portion of the data not considered during the fitting. This portion is related to the initial part of the loading, where a nonlinear relation between J and $CTOD$ exists . For example, the data

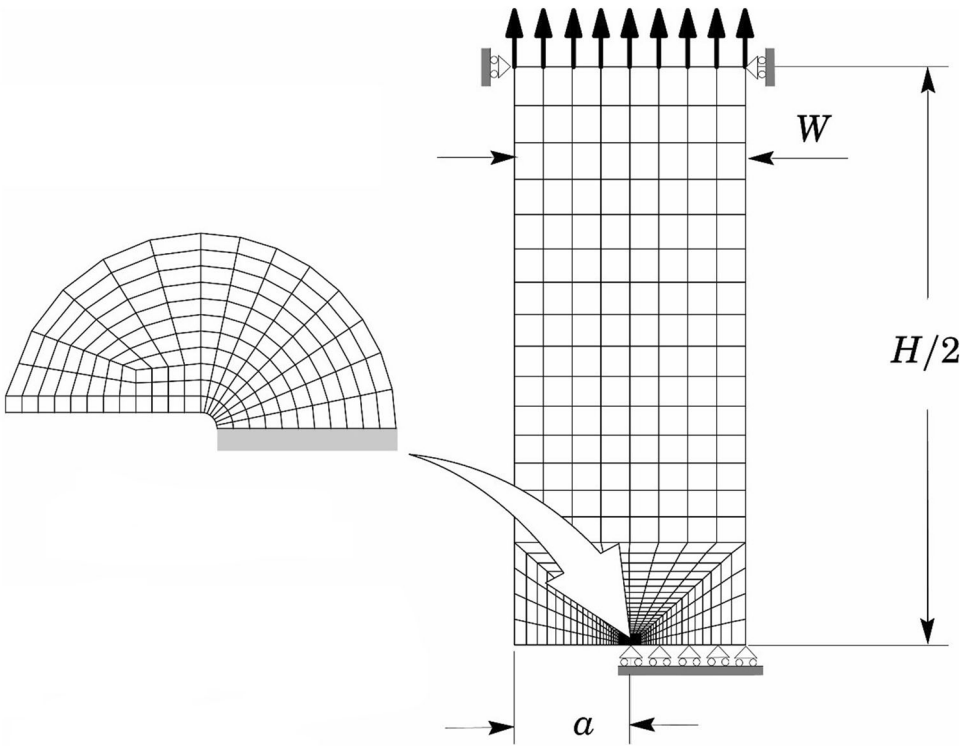

Fig. 5 Plane-strain finite element model for the clamped SE(T) specimen with $a/W = 0.5$

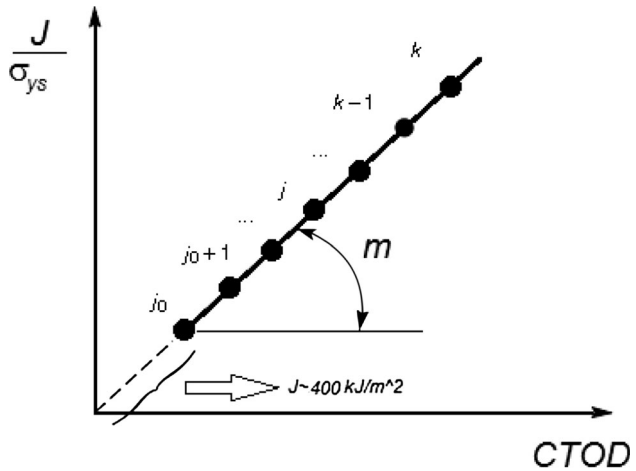

Fig. 6 Numerical determination of m values

until J values around 400 kJ/m^2 are excluded from the regression analysis for SE(B) specimens having moderate hardening coefficient ($n = 10$).

As described earlier, we want to check how precise are the m-equations developed in previous work [20] when compared to experimental predictions of J and CTOD parameters measured simultaneously for the same specimen.

4 Results

4.1 J–CTOD relationship in stationary cracks

The most important and relevant results from [20] are presented here. The reader is recommended to check this reference for further details. Figures 7 and 8 provide the variation in the J-integral with CTOD for the SE(B) and clamped SE(T) fracture specimens with different a/W-ratios and the moderate strain-hardening material ($n = 10$). The trends and results described here are essentially similar for other strain-hardening materials.

Consider first the J–CTOD relationship for the SE(B) geometry displayed in Fig. 7a. It can be seen that the J – CTOD relationship is relatively sensitive to a/W-ratio with increased levels of loading as measured by increased values of J. Figure 7b shows the evolution of parameter m with increased J for the analyzed SE(B) specimens. Here, the m-values display a strong variation at small levels of loading (as characterized by small J-values); such behavior derives directly from a strong nonlinear relationship between J and CTOD early in the loading of the specimen. After this transitional behavior, the m-values increase slowly with increased J and attain a constant value, albeit slightly dependent on the a/W-ratio, for larger levels of loading.

To provide a simple manipulation of the complete sets of results reported on [20], a functional dependence of

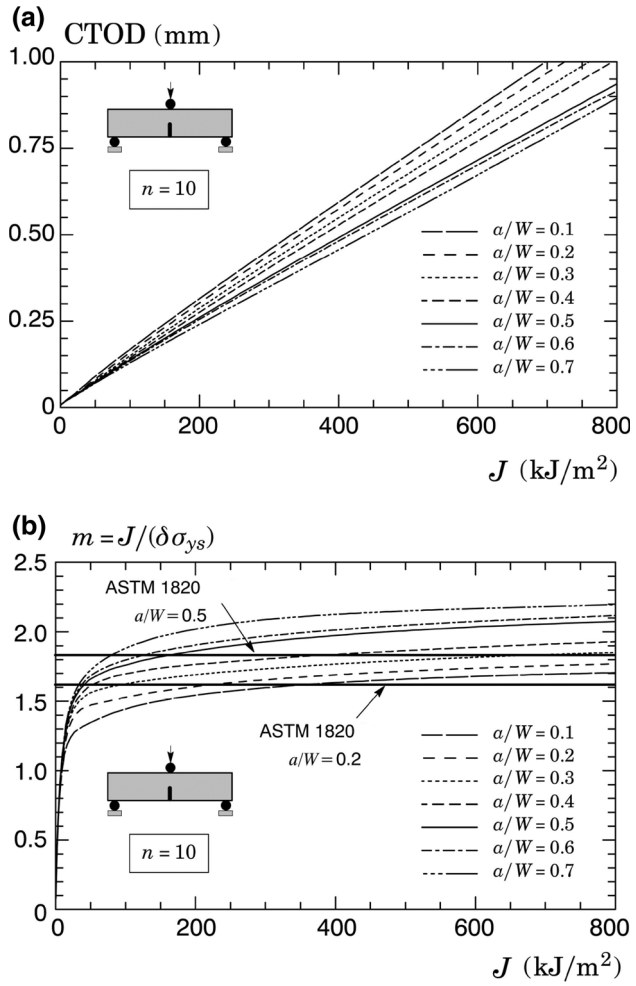

Fig. 7 J–CTOD relationship for the SE(B) specimen with varying a/W-ratio and $n = 10$ material derived from stationary crack analysis

parameter m with crack size, a/W, and hardening exponent, n, is obtained in the form:

$$m = h_1(a/W) + h_2(n) \tag{10}$$

where

$$h_1^{\mathrm{SEB}} = -0.194 + 1.077(a/W) - 0.238(a/W)^2 \tag{11}$$

$$h_2^{\mathrm{SEB}} = 14.391n^{-1} + 0.036n \tag{12}$$

and

$$h_1^{\mathrm{SET}} = 0.243 - 0.519(a/W) + 0.742(a/W)^2 \tag{13}$$

$$h_2^{\mathrm{SET}} = 11.545n^{-1} + 0.029n \tag{14}$$

where it is understood that a multivariate polynomial fitting is adopted to describe the coupled dependence of factor m on the a/W-ratio and hardening exponent n. The above expressions are valid in the range $0.2 \le a/W \le 0.7$, $5 \le n \le 20$, and $H/W = 10$ and $S/W = 4$ for SE(T) and SE(B) fracture specimens, respectively.

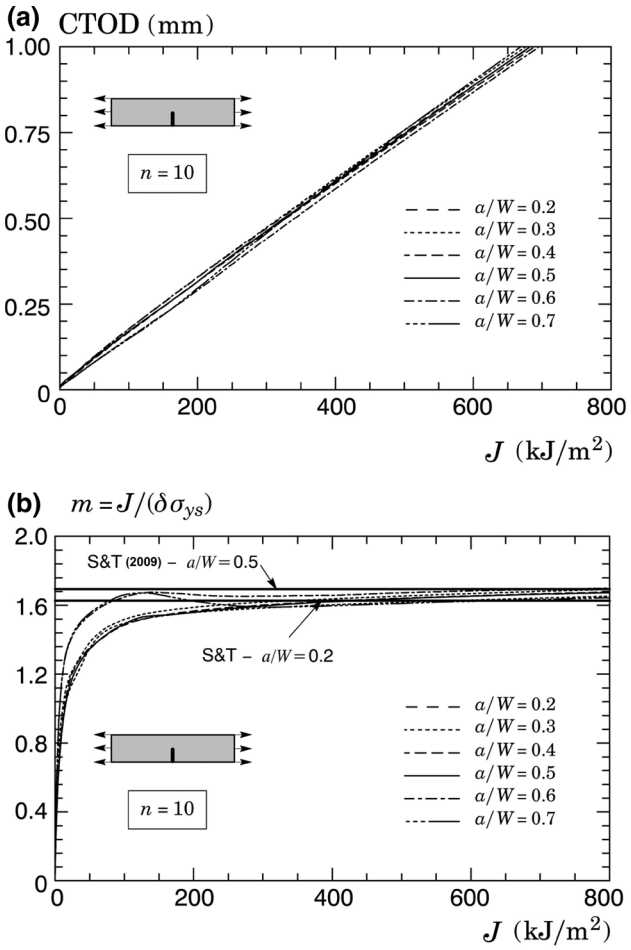

Fig. 8 J–CTOD relationship for the clamped SE(T) specimen with varying a/W-ratio and $n = 10$ material derived from stationary crack analysis

To facilitate comparisons with previous reported results for J–CTOD relationships in SE(B) and clamped SE(T) specimens, Figs. 7 and 8 also include the m-values derived from previous Eq. (10) for each crack configuration with $a/W = 0.2$ and 0.5 using the strain-hardening exponent of $n = 10$ for material employed in the numerical analyses. For the SE(B) specimen, Fig. 7 shows the m-values based on ASTM 1820 [4], whereas Fig. 8 displays m-values derived from 3D analyses of clamped SE(T) specimens performed by Shen and Tyson (S&T) [30]. It can be seen an overall good agreement between the presents results and the reported m-values from ASTM 1820 [4] and Shen and Tyson (S&T) [30].

Although an excellent agreement can be seen between the current m results and the reported m-values obtained by S&T' equation [30] and small differences, ~ 12 %, using the ASTM E1820 expression [4], a comparison of the m-values has to be done with special care because the m values have been normalized with respect to different reference stresses . The current m-values were based upon the use of σ_{ys} and [4] and [30] used σ_{flow} which is the average value between the 0.2 % offset yield

strength (σ_{ys}) and the ultimate tensile strength (σ_{TS}). σ_{flow} is typically used to include the influence of plastic yielding upon fracture test parameters.

Being δ inversely proportional to $m \cdot \sigma$, the plastic constraint factor (m) obtained via S&T [30] equation will produce δ estimations lower than current predictions made by Eq. (10). Even though the ASTM E1820 equation [4] produces m values lower than the current proposal, Eq. (10), the final δ value will depend on the material strain hardening. If $\sigma_{flow}/\sigma_{ys} > 1.12$, ASTM E1820-CTOD will be lower than the CTOD (δ) obtained by Eq. (10).

4.2 Experimental verification of J–CTOD relationship

The first set of results used to check the accuracy of Eq. (10) is taken from Moore and Pisarski [21]. They tested base metal pipeline steel grade API-5L X65 having a thickness $t = 23$ mm. A set of SE(T) specimens were extracted with dimensions 2BxB following the DNV-RP-F108 recommendations. The final width W was set as 19 mm, B=38mm. Three different sets of six specimens were tested with different nominal crack length-to-specimen width a/W ratios: 0.105, 0.3475, and 0.5475 [21]. For each set, six specimens were tested to different CMOD levels to generate data points for R curve by the multiple-specimen procedure as recommended by the DNV [12]. A double-clip gauge arrangement was used to measure the displacement at two different heights above the specimens surface. CTOD was estimated by Eq. (8). The J values were obtained by Eqs. (2)–(4), using the K and η equations given in DNV-RP-F108 [12].

The material has 528 MPa yield stress(σ_{ys}) and 610 MPa tensile strength (σ_{uts}) at room temperature (20°C) with low hardening properties ($\sigma_{uts}/\sigma_{ys} \approx 1.155$). The estimated strain-hardening exponent is $n = 16.63$ for the API X65 parent material.

Figures 9 and 10 show the evolution of J/σ_{ys} -ratio versus CTOD values for SE(T) specimens with $a/W = 0.348$ and $a/W = 0.548$, respectively, for different levels of remote loading and associated ductile crack growth. As can be seen, good predictions are made for the first points in each graph using Eq. (10).These good agreements are valid until J values around 900 and 700 kJ/m^2 for $a/W = 0.348$ and $a/W = 0.548$, respectively. These J values are associated with small amounts of crack growth. For very high levels of J , associated with $\Delta a > 0.5$ mm, the predicted values are not in good agreement with the measured values. Differences around 23 and 31 % are found for $a/W = 0.348$ and $a/W = 0.548$, respectively, at the maximum J value.

These results reveal that predicted instantaneous $((J_i/\sigma_{flow})/CTOD_i)$ m values are higher than experimental measured m values. It means that CTOD estimation using J

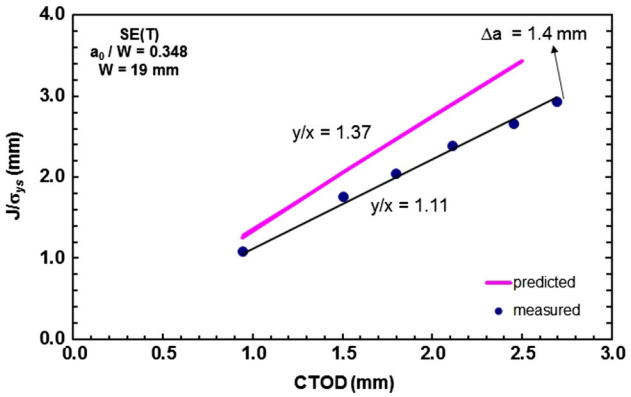

Fig. 9 Comparison between predicted and measured m parameter for SE(T) specimen made from API-5L X65 steel having $a/W = 0.348$

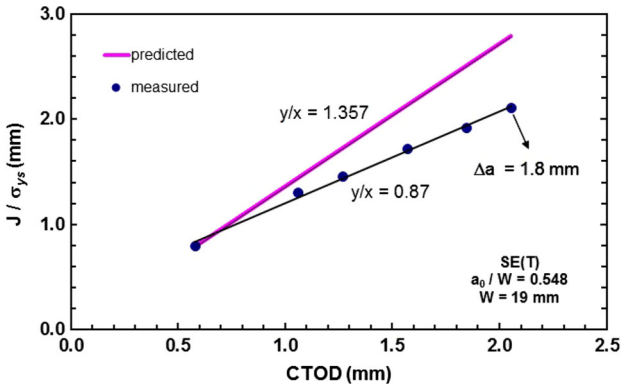

Fig. 10 Comparison between predicted and measured m parameter for SE(T) specimen made from API-5L X65 steel having $a/W = 0.548$

value will be conservative if CTOD value measured by double-clip gauge method is taken as the true physical displacement at the crack tip. We think that there are three possible sources causing the differences shown in Figs. 9 and 10, namely (i) experimental estimation of J Integral, (ii) CTOD definition, and (iii) strain-hardening estimation. First, the differences can be a consequence of the experimental procedure used to calculate the J-Integral. The used η_J factors of Eq. (4) are multiplied by a factor 0.85 resulting in reduced J values when compared to J values computed from the contour integral definition, see Anderson [2] for details of J as a path-independent line integral. This fact can explain partially the differences shown in Figs. 9 and 10.

Another point to take into account is the influence of the definition of CTOD. Definition of CTOD based on the 90° correlates well with Eq. (8) for small crack extension ($\Delta a \approx 1$ mm). Park et al. [31] provide some experimental data that show the agreement of both measures of CTOD for SE(T) specimens machined from X70 pipeline girth weld for small crack extension. The double-clip gauge approach provides larger values of CTOD for considerable

amount of crack growth. Therefore, this fact can be also responsible for the differences between predicted and measured constraint factors (m) for the SE(T) specimen as shown in Figs. 9 and 10.

Finally, a third factor contributing to differences in Figs. 9 and 10 may be attributed to the strain-hardening parameter used in Eq. (10). Moore and Pisarski [21] did not provide the specific strain-hardening exponent n for the API X65 material. The estimated strain-hardening exponent $n = 16.63$ was obtained by using the relationship between σ_{ys}/σ_{uts} and n proposed by the API 579 standard [32].

Additionally, a second set of experimental data is used to verify the accuracy of Eq. (10). The experimental data are taken from Pussegoda et al. [22]. Tests were based on procedures published by Det Norske Veritas [12]. They used the multiple-specimen technique using specimens of 2BxB cross section without side grooves and developed R curves from J and CTOD data using specimens of increasing crack size. Coupons were cut and machined from base metal steel grade 690, a pipe with nominal wall thickness $t = 19$ mm. The final specimen dimensions were $W = 17.5$ mm, $B = 35$ mm, and length $H = 10W$ with 90 mm for specimen grips on each side. A notch was introduced by EDM from the ID surface to a depth of 3.6 mm. All specimens were pre-cracked by fatigue until a target value $a/W = 0.34$.

For this set of data, six specimens were tested to different CMOD levels to generate data points for the R curve. J integral was calculated at the end of each test from the force and plastic component of the P-CMOD area according to the DNV procedure [12]. A double-clip gauge arrangement was used to measure the displacement at 2.4 and 12.4 mm above the specimens surface. CTOD was estimated using Eq. (8). The estimated yield stress and tensile strength for this material were $(\sigma_{ys}) = 623$ MPa and $(\sigma_{uts}) = 801$ at room temperature (20°C). The predicted strain-hardening exponent is $n = 11.2$ for the steel grade 690 using the relationship between σ_{ys}/σ_{uts} and n proposed by the API 579 standard [32].

Figure 11 shows the evolution of J/σ_{ys} -ratio versus CTOD values for the SE(T) specimen with $a_0/W = 0.34$ at different load levels. As can be seen, acceptable predictions are made in the whole range of CTOD values shown in Fig. 11. The difference between predicted and measured is around 12 % at low levels of J-Integral and 14 % for very high levels of J-Integral ($J_{max} = 1800\,kJ/m^2$). This J_{max} value is associated with considerable amounts of crack growth, $\Delta a \approx 1.7$ mm. Fig. 11 shows that experimental CTOD estimations based on the double-clip gauge method yield higher values than those measured numerically by the 90° procedure. Therefore, considering the δ value coming from the double-clip gauge method as representative of the vertical displacement at the crack tip, prediction of δ values will be conservative using Eq.10.

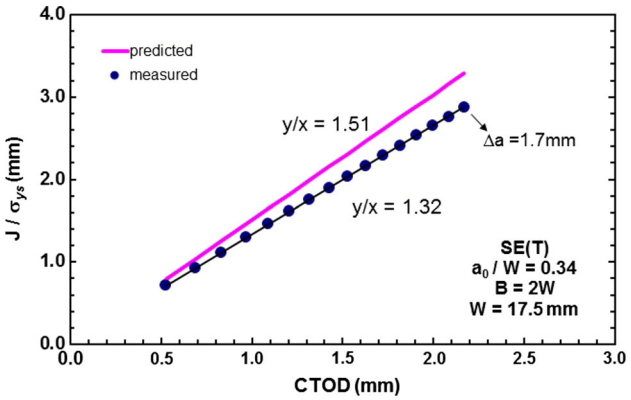

Fig. 11 Comparison between predicted and measured m parameter for SE(T) specimen made from steel grade 690 (×100) having $a/W = 0.34$

Regarding the experimental data for the SE(B) specimens, Aguirre and Ferreira [23] have carried out tests on a API-5L X65 steel sheet, with thickness equal to half inches in as-rolling condition. The SE(B) dimensions are as follows: width $W = 10$ mm, $B = 5$ mm and unsupported span $S = 55$ mm. The initial notch depth is 2 mm. All specimens were fatigue pre-cracked until a target value $a/W = 0.5$. Four specimens were tested by Aguirre and Ferreira [23] using the multiple-specimen approach. Each specimen was loaded until reaching a specified load level. The material has 504 MPa yield stress(σ_{ys}) and estimated strain-hardening exponent $n = 7.53$. The determination of J-Integral was made according to ASTM E 1820-01, and the CTOD was evaluated using the plastic hinge model.

Figure 12 shows the predicted and measured J/σ_{ys} -ratio versus CTOD values for the SE(B) geometry with $a/W = 0.5$. It is clear the perfect match between both curves is shown in Fig. 12. It is noteworthy to observe the very small amount of ductile crack growth achieved in this test, with $\Delta a_{max} = 0.5$ mm. For these particular data, the ductile crack growth effects on the J–CTOD relationship are minimal due to the small ductile extension during the tests. Thus, Fig. 12 suggests that Eq. 10 is a valid equation to correlate δ and J-Integral values for SE(B) geometries under small ductile crack extension.

The last set of experimental data used to validate Eq. 10 comes from Zerbst et al. [24]. The steel used in their study was a cold deformed 450 YS Thermomechanically Controlled Processed (TMCP) steel. SE(B) specimens were machined from the plates having L-S notch orientation. A multiple-specimen technique was followed to obtain the resistance (R) curve. A total of 20 specimens were machined and tested until attaining a specified CMOD value.

The J-Integral was evaluated using the seminal work of Kirk and Dodds [27], and the CTOD was obtained using the plastic hinge model as proposed in the ASTM E1290

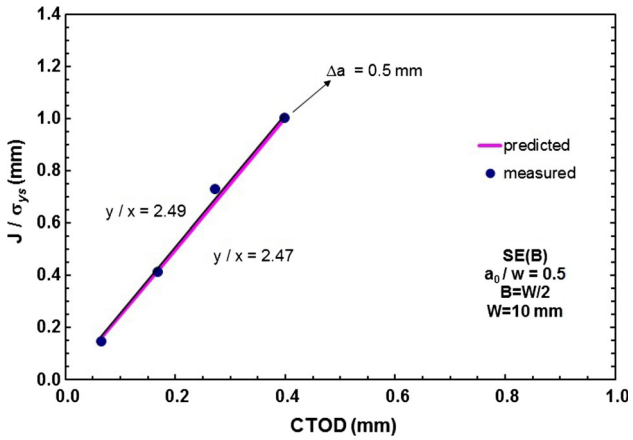

Fig. 12 Comparison between predicted and measured m parameter for SE(B) specimen made from API-5L X65 steel having $a/W = 0.5$

[5] standard from 1993. The measured yield stress and tensile strength for this material were $(\sigma_{ys}) = 420$ MPa and $(\sigma_{uts}) = 510$ at room temperature (20°C). The predicted strain-hardening exponent is $n = 13.45$ for the 450 YS steel using the relationship between σ_{ys}/σ_{uts} and n proposed by the API 579 standard [32]. Figure 13 shows the predicted and measured J/σ_{ys} -ratio versus CTOD values for the SE(B) geometry having $a_0/W = 0.5$.

An excellent agreement is observed for J values up to 500 kJ/m^2 that are associated with small crack growth (blunting line region) ($\Delta a < 0.4$ mm). For higher J values, ≈ 1130 kJ/m^2, a difference around 18 % can be measured between predicted and measured values. Therefore, for this specific study, reliable predictions of δ from J values can be made using Eq. 10 if small ductile crack growth is considered, i.e., $\Delta a < 0.5$ mm.

Figures 12 and 13 reveal that these experimental data are above the maximum J-Integral capacity for a specimen defined by the ASTM E1820-13 [4]. However, it is important to observe the highly linear relationship between

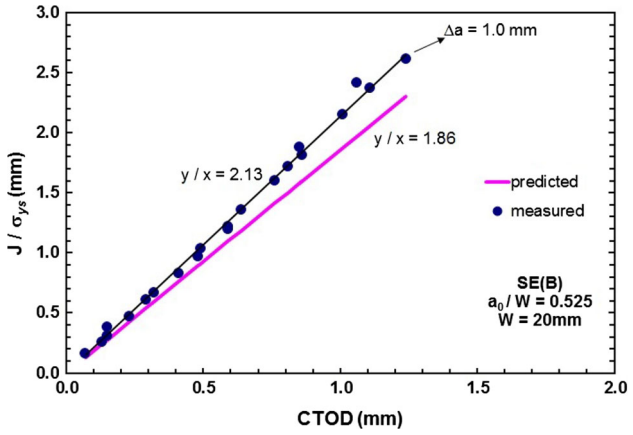

Fig. 13 Comparison between predicted and measured m parameter for SE(B) specimen made from 450 YS TMCP steel having $a/W = 0.5$

J and CTOD well beyond the limits established by [4] for both materials. Probably, the fracture conditions (stress–strain fields) are not well defined by the J-Integral alone. Thus, we cannot use the whole experimental data to represent the material toughness property. The data outside the ASTM limits may be geometry-dependent.

5 Concluding remarks

The extensive set of nonlinear finite element analyses for detailed plane-strain models of SE(B) and clamped SE(T) fracture specimens with varying crack sizes and strain-hardening properties developed in a previous work [20] provides the basis to determine accurate relationships between J and CTOD for use in testing protocols for toughness measurements. These analyses include stationary and crack growth plane-strain results to determine J and CTOD for SE(B) and clamped SE(T) cracked configurations based on load–displacement records.

The results described here clearly reveal that conservative estimations of the CTOD parameter can be made based on J values using the proposed J–CTOD relationships, Eq. 10, including small ductile crack growth. The current equations to estimate the plastic constraint parameter m are highly recommended for Δa lower than 0.5 mm. Current procedures to determine CTOD values from first evaluating the plastic component of J using the plastic work defined by the area under the load versus CMOD curve and then converting it into the corresponding value of plastic CTOD provide accurate measurements of crack growth response in terms of *CTOD-R* curves.

Acknowledgments This investigation is supported by Fundação de Amparo à Pesquisa do Estado de São Paulo Paulo (FAPESP) through research grant 2012/00094-2 and 2013/01139-2 provided to the first author (DFBS). The work of CR is supported by the Brazilian Council for Scientific and Technological Development (CNPq) through Grants 3041322009-8 and 4765812009-5.

References

1. J. Martin, R. Koers. Ctod versus j-integral as a fracture parameter (1998). URL www.eurofitnet.org
2. T.L. Anderson, *Fracture Mechanics: Fundaments and Applications*, 3rd edn. (CRC Press, Boca Raton, FL, 2005)
3. C. Wilson, J. Landes, J. Test. Eval. **22**, 505 (1994)
4. American Society for Testing and Materials. Standard test method for measurement of fracture toughness, ASTM E1820–2013 (2013)
5. ASTM, American Society for Testing and Materials, ASTM E1290 (2008)
6. T.L. Anderson, ASTM STP **945**, 741–753 (1988)
7. C. Shih, J. Mech. Phys. Solids **29**, 305 (1981)
8. R.M. McMeeking, D.M. Parks, Elastic–plastic fracture, in *ASTM STP*, ed. by J.D. Landes, J.A. Begley, G.A. Clarke (American

Society for Testing and Materials, Philadelphia, 1979), pp. 175–194
9. C.F. Shih, M.D. German, Int. J. Fract. **17**, 27 (1981)
10. DNV, Submarine pipeline systems. Tech. rep., Det Norsk Veritas, DNV-OS-F101 (2007)
11. S. Cravero, C. Ruggieri, Int. J. Fract. **148**, 347 (2007)
12. Det Norske Veritas. Fracture control for pipeline installation methods introducing cyclic plastic strain, DNV-RP-F108 (2006)
13. G. Shen, W.R. Tyson, J. Test. Eval. **37**(4), JTE102368 (2009)
14. B. Nyhus, State of the art for the use of SE(T) specimens to test fracture properties in pipes for reeling. Tech. rep., SINTEF Materials Technology (2001)
15. Method of test for determination of frature toughness in metallic materials using single edge notched tension (sent) specimens (2014)
16. D.Y. Park, W.R. Tyson, J.A. Gianetto, G. Shen, R.S. Eagleson, in *8th International Pipeline Conference (IPC)* (Calgary, Canada, 2010)
17. C. Ruggieri, Eng. Fract. Mech. **79**, 245 (2012)
18. M. Paredes, C. Ruggieri, Eng. Fract. Mech. **89**, 24 (2012)
19. W. Andrews, in *The Crack Tip Opening Displacement in Elastic-Plastic Fracture Mechanics*, ed. by K. Schwalbe (1985)
20. D.F.B. Sarzosa, C. Ruggieri, in *International Pipeline Conference (IPC)* (2014)
21. L.P. Moore, H. Pisarski, in *Twenty-two International Ocean and Polar Engineering Conference* (2012)
22. L. Pussegoda, W.R. Tyson, J. Gianetto, G. Shen, H. Pisarski, in *Twenty-third International Offshore and Polar Engineering* (ISOP, 2013)
23. I. Aguirre, I. Ferreira, in *Eighteen International Congress of Mechanical Engineering COBEM* (2005)
24. U. Zerbst, J. Heerens, K. Shchwalbe, Eng. Fract. Mech. **69**, 1093 (2002)
25. H. Tada, P.C. Paris, G.R. Irwin, *The Stress Analysis of Cracks Handbook*, 3rd edn. (American Society of Mechanical Engineers, New York, 2000)
26. S. Cravero, C. Ruggieri, Eng. Fract. Mech. **72**, 1344 (2005)
27. M.T. Kirk, R.H. Dodds, J. Test. Eval. **21**, 228 (1993)
28. A. Gullerud, K. Koppenhoefer, A. Roy, S. RoyChowdhury, M. Walters, R.J. Dodds, (2008)
29. C. Ruggieri, FRACTUS2D: numerical computation of fracture mechanics parameters for 2-D cracked solids. Technical report, University of Sao Paulo (2011)
30. G. Shen, W.R. Tyson, in *Pipeline Technology Conference (PTC 2009)* (Ostend, Belgium, 2009)
31. D. Park, J. Gravel, C. Simha, D.D. J. Liang, in *Pressure Vessels and Piping Conference, ASME* (July, 2014)
32. American Petroleum Institute. Fitness-for-service, API RP-579-1 / ASME FFS-1 (2007)